SCIENCE CHINA
Physics, Mechanics & Astronomy

• Article •

August 2021 Vol. 64 No. 8: 287412
https://doi.org/10.1007/s11433-021-1726-0

Structure and magnetic properties of the $S = 3/2$ zigzag spin chain antiferromagnet $BaCoTe_2O_7$

Lisi Li[1], Xunwu Hu[1], Zengjia Liu[1], Jia Yu[1], Benyuan Cheng[2,3], Sihao Deng[4], Lunhua He[4,5,6], Kun Cao[1], Dao-Xin Yao[1], and Meng Wang[1*]

[1] *Center for Neutron Science and Technology, School of Physics, Sun Yat-sen University, Guangzhou 510275, China;*
[2] *Shanghai Institute of Laser Plasma, Shanghai 201800, China;*
[3] *Center for High Pressure Science and Technology Advanced Research, Shanghai 201203, China;*
[4] *Spallation Neutron Source Science Center, Dongguan 523803, China;*
[5] *Beijing National Laboratory for Condensed Matter Physics, Institute of Physics, Chinese Academy of Sciences, Beijing 100190, China;*
[6] *Songshan Lake Materials Laboratory, Dongguan 523808, China*

Received February 16, 2021; accepted May 24, 2021; published online July 1, 2021

We report a study of the structure and magnetic properties of the $S = 3/2$ zigzag spin chain compound $BaCoTe_2O_7$. Neutron diffraction measurements show that it crystallizes in the noncentrosymmetric space group *Ama*2 with a canted ↑↑↓↓ spin structure along the quasi-one-dimensional zigzag chain and a moment size of 1.89(2) μ_B at 2 K. Both magnetic susceptibility and specific heat measurements yield an antiferromagnetic phase transition at $T_N = 6.2$ K. A negative Curie-Weiss temperature, $\Theta_{CW} = -74.7(2)$ K, and an empirical frustration parameter, $f = |\Theta_{CW}|/T_N \approx 12$, are obtained by fitting the magnetic susceptibility, indicating antiferromagnetic interactions and strong magnetic frustration. From ultraviolet-visible absorption spectroscopy and first-principles calculations, an indirect band gap of 2.68(2) eV is determined. We propose that the canted zigzag spin chain of $BaCoTe_2O_7$ may produce a change in the polarization via the exchange-striction mechanism.

antiferromagnet, zigzag spin chain, magnetic frustration, spin structure

PACS number(s): 75.50.Ee, 75.10.Pq, 75.30.Gw, 61.12.Ld

Citation: L. Li, X. Hu, Z. Liu, J. Yu, B. Cheng, S. Deng, L. He, K. Cao, D.-X. Yao, and M. Wang, Structure and magnetic properties of the $S = 3/2$ zigzag spin chain antiferromagnet $BaCoTe_2O_7$, Sci. China-Phys. Mech. Astron. **64**, 287412 (2021), https://doi.org/10.1007/s11433-021-1726-0

1 Introduction

Quasi-one-dimensional (1D) systems have been extensively studied due to their intriguing properties [1-5].

Although an ideal 1D system does not become magnetically ordered at finite temperature [6], interchain interactions are inevitable in a real 1D material, which can result in a 3D magnetically ordered ground state [5].

Moreover, magnetic anisotropy arising from spin orbital coupling and crystal field environment constitute additional degrees of freedom that influence the magnetic order of a 1D system. In a spin-3/2 Co^{2+} based 1D system, rich phase diagrams and certain emergent phenomena appear in a magnetic field or at high pressure owing to its strong magnetic anisotropy. Complicated magnetic field induced phase diagrams were observed in the Co^{2+} based Ising spin chain systems $BaCo_2V_2O_8$ [7, 8] and $CoNb_2O_6$ [9, 10]. A plateau was

*Corresponding author (email: wangmeng5@mail.sysu.edu.cn)

observed in the magnetization of the spin chain systems α-CoV_2O_6 [11, 12] and $Ca_3Co_2O_6$ [13, 14]. Thus, for a Co^{2+}-based 1D system, a combination of intra-and inter-chain interactions and magnetic anisotropy can produce various magnetic properties. It is therefore interesting to explore the exotic physics underlying the magnetic behaviors of the Co^{2+}-based 1D systems.

Compounds with the chemical formula $BaMTe_2O_7$ (M=Cu, Zn, Mg) belong to 1D chain systems that crystallize in the noncentrosymmetric space group *Ama*2 (Space group No. 40) [15, 16]. Their structures comprise a zigzag-chain arrangement of the transition metal atoms M within the crystal field environment of the complex MO_5, in which the MO_5 entities are not directly connected by O^{2+}, as shown in Figure 1(a). The compounds $BaMTe_2O_7$ (M = Zn, Mg) are nonmagnetic [16]. Although the spin of Cu^{2+} is 1/2 in $BaCuTe_2O_7$, no magnetic order has been detected down to 1.8 K [15]. The similar Co^{2+} based zigzag spin chain compounds α-$BaCoX_2O_7$ (X=P, As) have been investigated extensively [17, 18]. They exhibit antiferromagnetic (AFM) orders below T_N=11 and 10 K, respectively. The susceptibility of α-$BaCoX_2O_7$ exhibits a large magnetic anisotropy. Their magnetization exhibits a 1/3 plateau below T_N, which results from the incommensurate atomic shifts. Because of the fascinating magnetic properties of the Co^{2+} based zigzag spin chain systems, it is interesting to examine the properties of $BaCoTe_2O_7$. To our knowledge, there are no previous reports of the synthesis and characterization of $BaCoTe_2O_7$.

In this study, magnetic susceptibility, magnetization, specific heat, neutron powder diffraction (NPD), and ultraviolet-visible (UV-vis) absorption spectroscopy measurements as well as first-principles density functional theory (DFT) calculations were performed to determine the properties of $BaCoTe_2O_7$. A canted ↑↑↓↓ spin structure is identified below T_N = 6.2 K, with a propagation vector $\boldsymbol{k}$ = (0.5, 0, 0). A negative Curie-Weiss temperature Θ_{CW} = −74.7(2) K is obtained by fitting the susceptibility, which indicates that AFM interactions dominate. Large anisotropy is revealed on in the susceptibility and magnetization measurements. An indirect bandgap is determined as of 2.68(2) eV. The ordered moment of Co^{2+} may be reduced by covalency between the Co^{2+} 3d and O^{2-} 2p orbitals and magnetic frustration.

2 Experiments and calculations

Single-crystal samples of $BaCoTe_2O_7$ were grown in two steps. First, a polycrystalline sample was synthesized using the conventional solid-state reaction. The starting materials $BaCO_3$ (99.99%), Co_3O_4 (99.9%), and TeO_2 (99.99%) were mixed thoroughly in the stoichiometric ratio in an agate mortar. The mixed powders were then pressed to a pellet and put into an alumina crucible covered with a lid. The pellet was calcined at 650°C in air in a muffler furnace for 7 d with several intimidate grindings. Second, single-crystal samples were grown using the flux method. NaCl and KCl mixed in a 1:1 molar ratio were used as fluxes. The $BaCoTe_2O_7$ powder samples and fluxes with a weight ratio 1:0.75 were placed to an alumina crucible. The mixtures were heated to 800°C within 6 h and dwelled for 24 h. After then, it was cooled to 650°C at 1°C/h then down to room temperature by tuning off the muffler furnace. The flux was washed with hot water. Single-crystal X-ray diffraction (XRD) measurements were performed on a SuperNova (Rigaku) single-crystal X-ray diffractometer.

Our NPD experiment was conducted on the general pur-

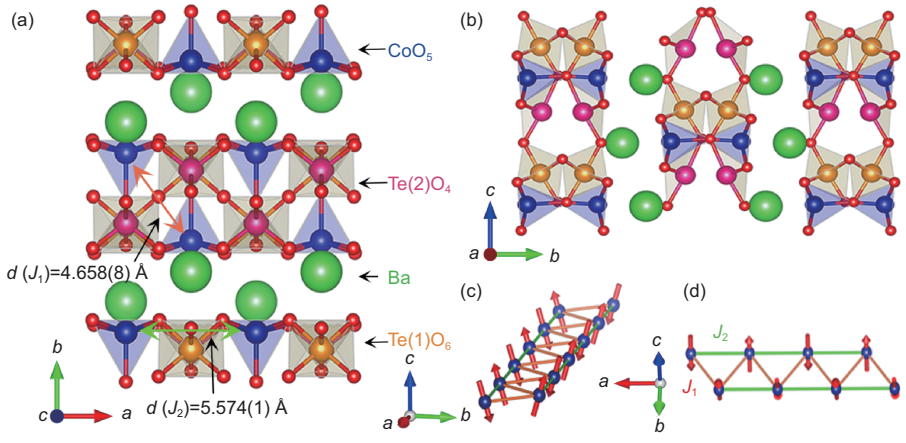

Figure 1 (Color online) The crystal structure of $BaCoTe_2O_7$ viewed along (a) the c and (b) the a directions. (c), (d) Different views of the magnetic structure and exchange-interaction network in a zigzag chain. The CoO_5, $Te(1)O_6$ and $Te(2)O_4$ complexes and the Ba atoms are shown in different colors. The paths of intrachain interactions J_1 and J_2 are colored in orange and green, respectively. The red arrows represent the spin directions.

pose powder diffractometer (GPPD) installed at the China Spallation Neutron Source (CSNS) [19]. The powder samples of $BaCoTe_2O_7$ were filled in a cylindrical vanadium can and measured at 2 and 300 K. The Rietveld method was employed to refine the NPD patterns using the *FullProf* suit package [20]. DC susceptibility and specific heat data were collected on a commercial physical property measurement system (PPMS, Quantum Design). The direction of the single crystal was determined by an X-ray Laue diffractometer. UV-vis spectroscopy measurements were conducted on an Ocean Optics DH-2000-BAL spectrometer.

We performed DFT calculations using the projector augmented wave [21] method with the generalized gradient approximation (GGA) of Perdew-Burke-Ernzerhof [22] functional as implemented in the Vienna *ab initio* simulation package [23,24]. The kinetic cutoff energy was set to 550 eV and Γ-centered Monkhorst-Pack meshes of $2\times2\times3$ was used for the Brillouin-zone integrations [25]. For comparison with experiment, the lattice constants and spin structure refined from NPD at 2 K were employed. The atomic positions were fully relaxed using a conjugated gradient algorithm until the remaining force on each atom was < 0.01 eV/ Å. Spin-orbit coupling was considered in all the calculations. Moreover, we calculated the free energies of the different magnetic configurations.

3 Results and discussion

Figure 2 shows the observed and calculated NPD patterns of $BaCoTe_2O_7$. The refined structures reproduce the NPD patterns at 300 and 2 K very well when magnetic reflections are considered. No impurity phase is found. Our refinement reveal that $BaCoTe_2O_7$ crystallizes in the space group *Ama*2, which is isostructural to $BaMTe_2O_7$ (M=Cu, Zn, Mg). Table 1 lists the structural parameters obtained at 2 K. The composition from the NPD refinement is $BaCo_{0.97}Te_{1.9}O_{6.64}$, close to the stoichiometric content. The refined parameters at 300 K are presented in the Supporting Information. As shown in Figure 1, each magnetic Co^{2+} ion is surrounded by five O^{2-} anions, thus forming a CoO_5 square pyramidal crystal field environment. The Te atoms exist in two valence states, $Te(1)^{6+}$ and $Te(2)^{4+}$, which yield the $Te(1)O_6$ and $Te(2)O_4$ crystal-field environments, respectively. The CoO_5, $Te(1)O_6$, and $Te(2)O_4$ entities are lined up in a zigzag chain running along the *a* direction. Along the *b* direction, Ba^{2+} ions separate the two dimensional $[CoTe_2O_7]^{2-}$ layers. In the *c* direction, three zigzag chains stack as a periodic sequence of CoO_5, $Te(1)O_6$, and $Te(2)O_4$. This crystal structure was then confirmed by a single crystal XRD experiment (see the Supporting Information).

By comparing NPD patterns at 300 and 2 K, reflections from magnetic scattering can be clearly identified in Figure 2(b). All these magnetic peaks can be indexed with a propagation vector $\boldsymbol{k}$ = (0.5, 0, 0). A representational analysis was performed to determine the spin structure quantitatively using BasIreps in the *FullProf* suite package [26, 27]. This results in the non-zero irreducible representation (IR) Γ_1. One Co^{2+}-ion crystallographic site is splitted into two sites $Co^{2+}(1)$ (x, y, z) and $Co^{2+}(2)$ $(-x+1, -y+1/2, z-1/2)$. Table 2 lists the basis vectors (BV) for the two Co^{2+} sites of the IR Γ_1. The refinement with the IR Γ_1 reproduces the magnetic peaks at 2 K well, with the magnetic R factor R_{mag} = 4.27%. Consequently, the components of the magnetic moment along the *a*, *b*, and *c* directions are m_a = 0(0.1), m_b=0.60(4), and m_c=

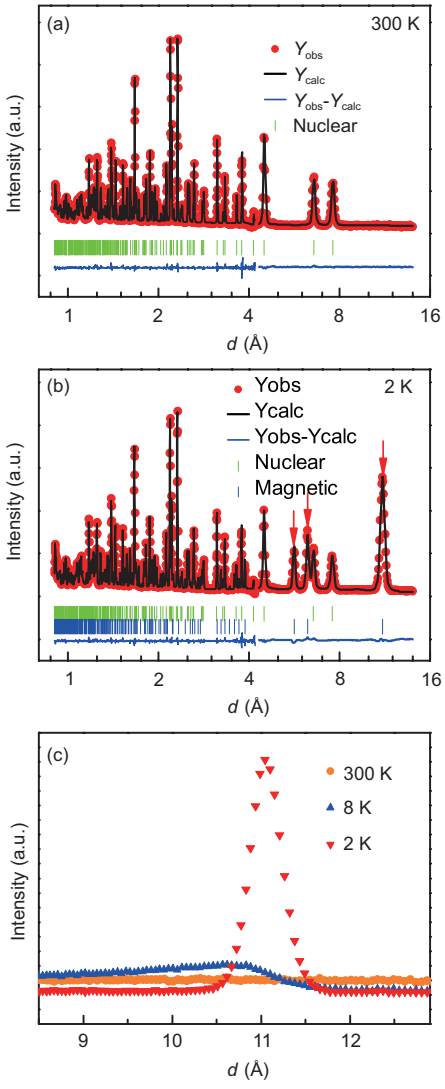

Figure 2 (Color online) Observed and calculated NPD patterns of $BaCoTe_2O_7$ at (a) 300 and (b) 2 K. (c) A magnified version of the NPD pattern in the range from 8 to 12.5 Å.

Table 1 Atoms, Wyckoff sites, fractional atomic coordinates $(x/a, y/b, z/c)$, and occupations of $BaCoTe_2O_7$ at 2 K. The numbers in the brackets are the corresponding errors. The refined lattice constants are a = 5.5685(1), b = 15.1449(4), and c = 7.2750(2) Å and the profile parameters are $R_p = 4.83\%, R_{wp} = 4.68\%, R_e = 1.75\%$, and $\chi^2 = 7.19$

Atoms	Wyckoff site	x/a	y/b	z/c	Occupation
Ba	4*b*	1/4	0.2083(2)	0.003(1)	1.0
Co	4*b*	1/4	0.1246(3)	0.519(2)	0.97(2)
Te1	4*b*	1/4	0.9230(2)	0.765(1)	0.95(2)
Te2	4*b*	3/4	0.0719(2)	0.250(1)	0.95(2)
O1	4*b*	3/4	0.1349(1)	0.006(1)	0.97(1)
O2	8*c*	0.0028(8)	0.1438(1)	0.3115(9)	1.98(3)
O3	4*b*	1/4	0.9856(2)	0.5357(8)	0.93(2)
O4	8*c*	0.0065(8)	0.8428(1)	0.6935(9)	1.85(3)
O5	4*a*	0	0	0.877(1)	0.91(2)

Table 2 Basis vectors of the magnetic Co sites with the propagation vector $\boldsymbol{k}$=(0.5,0,0). The atom sites of Co(1) and Co(2) are (x, y, z) and $(-x+1, -y+1/2, z-1/2)$, respectively

IR	BV	Co(1)	Co(2)
Γ_1	ψ_1	[1,0,0]	[−1,0,0]
	ψ_2	[0,1,0]	[0,−1,0]
	ψ_3	[0,0,1]	[0,0,1]

1.79(2) μ_B, thus yielding a total magnetic moment m_{tot} = 1.89(2) μ_B. Figure 1(c) and (d) show different views of the spin structures so determined. The spins are arranged within the *bc* plane perpendicular to the zigzag-chain direction. Along the zigzag chain, adjacent spins are oriented at a relative angle of 37° and are arrayed in an alternating ferromagnetic (FM) and AFM way, which can be recognized as a canted ↑↑↓↓ spin structure. Moreover, a similar magnetic structure, but with the only component of the magnetic moment oriented along the *c*-axis, is also tested; this yields m = 1.86(1) μ_B and R_{mag} = 4.69%, which is worse than that for the canted spin structure. Figure 2(c) shows the NPD patterns for a magnetic peak at 2, 8, and 300 K. The broad peak at 8 K, which is above the Néel temperature, suggests the existence of magnetic frustration and short range magnetic correlations.

Figure 3(a) shows temperature dependence of the magnetic susceptibility χ measured under zero-field cooling (ZFC) and field cooling (FC) on a powder sample of $BaCoTe_2O_7$. No obvious difference is found between the ZFC and FC data. There is a broad peak around $T_{max} \approx$ 20 K; this is a commonly observed characteristic for a 1D magnet because of the presence of magnetic correlations [5]. In the derivative $d\chi/dT$ shown in the inset of Figure 3(a), a peak appears at T_N = 6.2 K, which can be attributed to an AFM phase transition. Fitting the inverse susceptibility $1/(\chi - \chi_0)$ over the temperature range from 100 to 300 K to the Curie-Weiss law, $\chi = \chi_0 + C/(T - \Theta_{CW})$, yields the red solid line in Figure 3(a). The fitting shows that the contributions of core diamagnetism and Van Vleck paramagnetism χ_0 amount to $-7.63(8) \times 10^{-4}$ emu Oe^{-1} mol^{-1}, the Curie constant C is 4.22(1) emu K mol^{-1} Oe^{-1}, and the Curie-Weiss temperature Θ_{CW} is −74.7(2) K. The negative value of Θ_{CW} demonstrates that AFM interactions dominate in the system. An empirical formula for the frustration parameter is $f = |\Theta_{CW}|/T_N = 12.08 > 10$, which suggests the possible existence of magnetic frustration or the effect of low dimensionality [28]. The effective magnetic moment is estimated to be μ_{eff} = 5.77(1) μ_B, which is larger than that of the theoretical value of $\mu_{eff} = g\sqrt{S(S+1)}$ = 3.87 μ_B for a S = 3/2 system when assuming zero orbital residual and g = 2. The results signal a considerable orbital contribution from the Co^{2+} ions, consistent with the reports for other Co^{2+} based materials, such as $BaCoX_2O_7$ (X = P, As) [18], $Na_3Co_2SbO_6$ [29], $BaCo_2(AsO_4)_2$ [30].

Figure 3(b) and (c) present temperature dependence of the magnetic susceptibility χ and field dependent magnetization M measured in the different crystallographic directions of a single crystal of $BaCoTe_2O_7$. The susceptibilities measured with the magnetic field applied along the a direction (χ_a), the b direction (χ_b), and the c direction (χ_c) exhibit a phase transition at $T_N \approx$ 6 K, as seen in the derivative $d\chi/dT$, in agreement with that measured from the powder sample. In addition, these data exhibit large differences across the whole temperature range. For an isotropic 3D antiferromagnet, χ_a, χ_b, and χ_c should coincide in the high temperature range ($T > T_N$) [31]. The large anisotropy between χ_a, χ_b, and χ_c may be attributed to the anisotropy of the spin correlations persisting above T_N and the 1D nature of $BaCoTe_2O_7$. For example, the Co^{2+} based 1D compounds $BaCoP_2O_7$ [17], $Ba_2CoSi_2O_7$ [32], and $BaCo_2V_2O_8$ [7] also exhibit large anisotropies. The kinks in χ_a and χ_b at ~13 K in Figure 3 (b) may be related to impurities in the sample caused by contamination during the single-crystal growth process. The magnetization M_c measured with a magnetic field applied along the c direction exhibits a sharp change around

$\mu_0 H_c = 6$ T, while there are no anomalies in M_a and M_b. This is consistent with a spin flop-like transition for spins aligned in the bc plane with a dominant moment component m_c.

Figure 4 shows temperature dependence of the specific heat C_p measured under zero and a finite magnetic field on a pellet pressed from a powder sample of $BaCoTe_2O_7$. A λ-like phase transition is observed at $T_N = 6.2$ K, consistent with the susceptibility measurements shown in Figure 3. To estimate the magnetic contribution $C_{p,\mathrm{mag}}$ on the specific heat, we subtracted the phonon part $C_{p,\mathrm{ph}}$ from the total C_p; the electronic contribution is not considered because $BaCoTe_2O_7$ is an insulator. A modified Debye model is taken into account to estimate the phonon contribution, considering two phonon spectra: one being the spectrum of the light atoms (O^{2-}) and

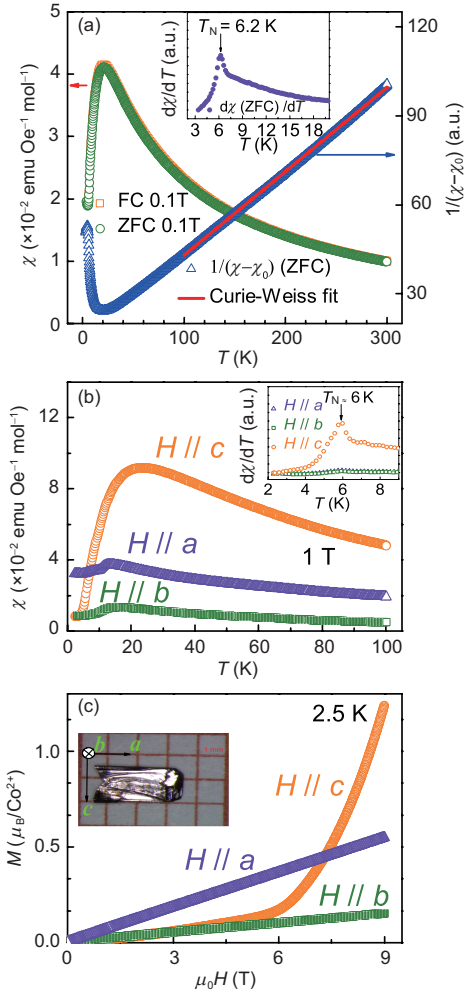

Figure 3 (Color online) (a) Left axis: temperature dependence of the susceptibility χ measured on a powder sample of $BaCoTe_2O_7$; the inset shows its derivative $d\chi/dT$. Right axis: inverse susceptibility $1/(\chi - \chi_0)$ and the Curie-Weiss fit. (b) Temperature dependence of χ measured along the three crystallographic directions of a single crystal; the inset shows their derivatives $d\chi/dT$. (c) Magnetization measured in the three crystallographic directions of a single crystal; the inset shows an image of the single crystal with the crystallographic directions indicated.

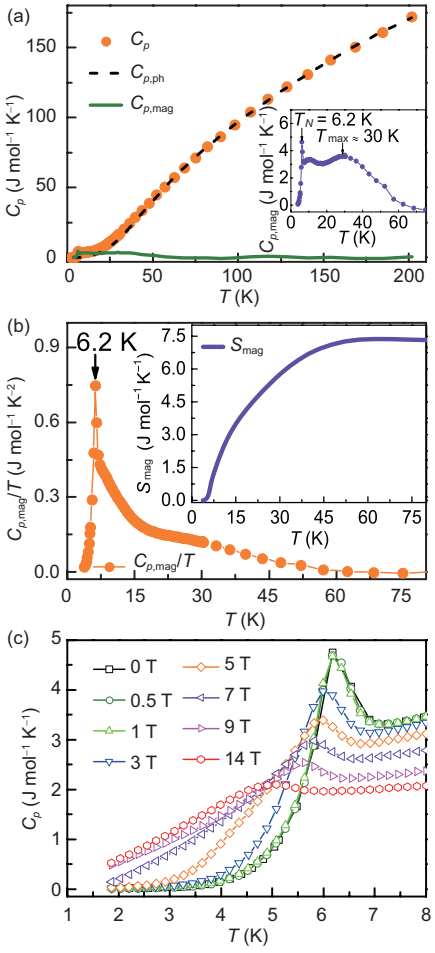

Figure 4 (Color online) (a) Temperature dependence of the total specific heat C_p, the phonon part $C_{p,\mathrm{ph}}$, and the magnetic part $C_{p,\mathrm{mag}}$ of $BaCoTe_2O_7$. The inset shows a magnified image of $C_{p,\mathrm{mag}}$ at low temperature. (b) Derived $C_{p,\mathrm{mag}}/T$ against temperature with the inset showing the magnetic entropy. (c) Specific heat C_p measured in different applied magnetic fields over the temperature range of 1.8-8 K.

the other the spectrum of the heavy atoms (Ba^{2+}, Co^{2+}, Te^{4+}, and Te^{6+}). This method was confirmed to be effective for analyzing M_2MnTeO_6 (M =Sr, Ba) [33, 34]. The formula for the modified Debye model is

$$C_{p,\mathrm{ph}} = 9R \sum_{n=1}^{2} C_n \left(\frac{T}{\Theta_{Dn}}\right)^3 \int_0^{\Theta_{Dn}/T} \frac{x^4 e^x}{(e^x - 1)^2} dx. \quad (1)$$

Fitting eq. (1) to the raw data over the temperature range from 60 to 200 K yields 6.5 light atoms and 4.5 heavy atoms out of the 11 atoms in a formula unit of $BaCoTe_2O_7$. The Debye temperatures, corresponding to the light and heavy atoms, are $\Theta_{D1} = 855(26)$ K and $\Theta_{D2} = 256(7)$ K, respectively. This atomic ratio is in good agreement with the 7 light atoms (O^{2-}) and 4 heavy atoms (Ba^{2+}, Co^{2+}, Te^{4+}, and Te^{6+}) in a formula unit of $BaCoTe_2O_7$. Based on the fitted parameters, the phonon part $C_{p,\mathrm{ph}}$ of the specific heat is extrapolated to 1.8 K, as shown by the black dashed line plotted in Figure

4(a). The magnetic part $C_{p,\mathrm{mag}}$ of the specific heat is obtained accordingly and is shown as the green solid line. A broad peak in $C_{p,\mathrm{mag}}$, with a maximum at ~ 30 K as shown in the inset of Figure 4(a), reveals the persistence of magnetic correlations above T_N, consistent with the magnetic susceptibility measurements shown in Figure 3. The magnetic entropy contribution to the magnetic state changes can be deduced from the formula $S_\mathrm{mag} = \int (C_{p,\mathrm{mag}}/T)\mathrm{d}T$. As shown in Figure 4(b), the magnitude of the resulting magnetic entropy at 80 K, S_mag = 7.38 J/(mol K)$^{-1}$, is lower than that given by the theoretical formula, $S_\mathrm{mag} = R\ln(2S+1)$ = 11.52 J/(mol K)$^{-1}$, for a magnetic correlation free Co^{2+} ion in the spin-only $S = 3/2$ case. The reduced value of S_mag can be attributed to the reduction of the ordered moment and to the persistence of magnetic correlations above T_N. Figure 4(c) shows the magnetic-field dependence of the Néel temperature, with T_N shifting toward lower temperatures with an increase in magnetic fields. A similar behavior has been observed in the zigzag chain antiferromagnet $BaNd_2O_4$ [35].

To obtain a better insight into the experimental results, we performed DFT calculations to examine the electronic structure and magnetism of $BaCoTe_2O_7$. The band gap is 2.68(2) eV, as determined from the UV-vis absorption spectrum. Accordingly, we selected a Coulomb repulsive U of 6 eV. Figure 5 shows the calculated density of states (DOS) and the electronic band structure of $BaCoTe_2O_7$. In Figure 5(a), it is shown that both the partial DOS of Co^{2+} and O^{2-} have significant contributions in the energy range of $-5 \le E \le -1$ eV, indicating covalency between the 3d orbitals of Co^{2+} and 2p orbitals of O^{2-}. The energy for the AFM ↑↑↓↓ spin structure, –5.8146 eV/atom, is lower than that of the FM spin structure, –5.7801 eV/atom.

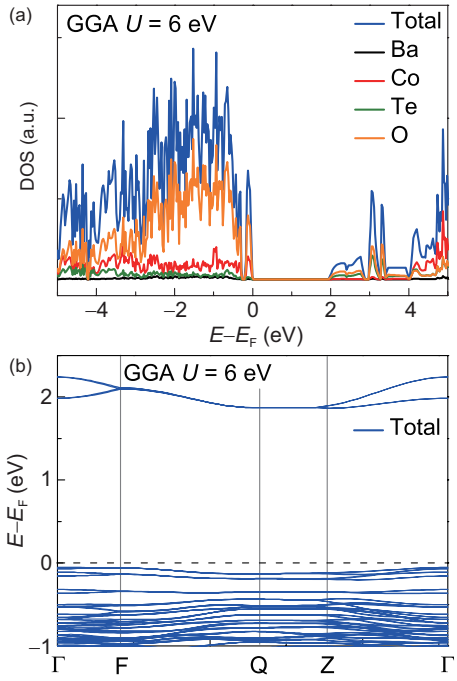

Figure 5 (Color online) (a) Calculated total and partial DOS for $BaCoTe_2O_7$ and (b) the band structure based on the experimentally determined magnetic structure and U = 6 eV.

The calculated ordered moments are $m_a = 0$, $m_b = 0.89$, $m_c = 2.66$, and $m_\mathrm{tot} = 2.80\ \mu_\mathrm{B}$, assuming the experimentally determined spin structure. The calculated ordered moment is smaller than the ideal local moment of 3 μ_B for Co^{2+} with a $3d^7$ electronic configuration, which may be attributed to the covalency. But it is considerably larger than the experimental result. The Co^{2+} ions in $BaCoTe_2O_7$ arrange in a triangular lattice in the zigzag chain and the competition between the intrachain exchange interactions J_1 (d=4.658(8) Å at T=2 K) and J_2 (d=5.574(1) Å at T=2 K) may lead to strong magnetic frustration, resulting in the reduced moment 1.89(2) μ_B as observed in experiment. Note that weak interchain exchange interactions J_3 are necessary to stabilize the long range magnetic order.

The noncentrosymmetric $BaCoTe_2O_7$ is pyroelectric in its paramagnetic phase, but not ferroelectric. Because its polarization can not be reversed by an applied electric field [15, 16]. However, in the magnetically ordered phase, the spin structure with alternative FM and AFM arrangements may reduce the symmetry and result in a change in the electric polarization ΔP along the chain direction by inducing different exchange striction on the ↑↑ and ↑↓ spin pairs. ΔP may be partially reversible, which then presents a scenario similar to type II multiferroics [36-41]. Therefore, it is important to explore the magnetoelectric coupling in $BaCoTe_2O_7$, which we will leave for future work.

4 Conclusions

To summarize, we synthesized both powder and single-crystal samples of $BaCoTe_2O_7$ and investigated its structure, magnetic, and electronic properties. An antiferromagnetic ↑↑↓↓ spin structure with a propagation vector $\boldsymbol{k} = (0.5, 0, 0)$ is revealed below T_N = 6.2 K. The large magnetic anisotropy at high temperatures suggests the existence of the magnetic exchange interactions above T_N. This field-induced behavior can be attributed to the effects of the single-ion anisotropy, the magnetic exchange interactions of Co^{2+}, as well as the 1D nature of this compound. Our DFT calculations suggest the existence of covalency between the Co^{2+} 3d and O^{2-} 2p orbitals. The covalency and magnetic frustration in the system may reduce its ordered moment. Further investigations on the spin dynamics and multiferroics in $BaCoTe_2O_7$ are necessary to revel its unique magnetic and electric properties.

Meng Wang was supported by the National Natural Science Foundation of China (Grant No. 11904414), and the National Key Research and Development Program of China (Grant No. 2019YFA0705702). Dao-Xin Yao was supported by the National Key Research and Development Program of China (Grant Nos. 2018YFA0306001, and 2017YFA0206203), the National Natural Science Foundation of China (Grant No. 11974432), the Guangdong Basic and Applied Basic Research Fund (Grant No. 2019A1515011337), and the Leading Talent Program of Guangdong Special Projects. We thank Hanjie Guo for the Laue measurements.

Supporting Information

The supporting information is available online at phys.scichina.com and link.springer.com. The supporting materials are published as submitted, without typesetting or editing. The responsibility for scientific accuracy and content remains entirely with the authors.

1 E. Ising, Z. Physik **31**, 253 (1925).
2 W. Heisenberg, Z. Physik **49**, 619 (1928).
3 H. Bethe, Z. Physik **71**, 205 (1931).
4 I. Affleck, J. Phys.-Condens. Matter **1**, 3047 (1989).
5 H.-J. Mikeska, and A. K. Kolezhuk, Lect. Notes Phys. **645**, 1 (2004).
6 N. D. Mermin, and H. Wagner, Phys. Rev. Lett. **17**, 1133 (1966).
7 Z. He, T. Taniyama, T. Kyômen, and M. Itoh, Phys. Rev. B **72**, 172403 (2005).
8 B. Grenier, V. Simonet, B. Canals, P. Lejay, M. Klanjšek, M. Horvatić, and C. Berthier, Phys. Rev. B **92**, 134416 (2015), arXiv: 1508.01815.
9 C. Heid, H. Weitzel, P. Burlet, M. Bonnet, W. Gonschorek, T. Vogt, J. Norwig, and H. Fuess, J. Magn. Magn. Mater. **151**, 123 (1995).
10 C. Heid, H. Weitzel, P. Burlet, M. Winkelmann, H. Ehrenberg, and H. Fuess, Phys. B-Condens. Matter **234-236**, 574 (1997).
11 M. Lenertz, J. Alaria, D. Stoeffler, S. Colis, and A. Dinia, J. Phys. Chem. C **115**, 17190 (2011).
12 C. B. Liu, Z. Z. He, S. L. Wang, M. Yang, Y. Liu, Y. J. Liu, R. Chen, H. P. Zhu, C. Dong, J. Z. Ke, Z. W. Ouyang, Z. C. Xia, and J. F. Wang, J. Phys.-Condens. Matter **31**, 375802 (2019).
13 A. Maignan, C. Michel, A. C. Masset, C. Martin, and B. Raveau, Eur. Phys. J. B **15**, 657 (2000).
14 S. Agrestini, L. C. Chapon, A. Daoud-Aladine, J. Schefer, A. Gukasov, C. Mazzoli, M. R. Lees, and O. A. Petrenko, Phys. Rev. Lett. **101**, 097207 (2008), arXiv: 0807.4489.
15 J. Yeon, S. H. Kim, M. A. Hayward, and P. S. Halasyamani, Inorg. Chem. **50**, 8663 (2011).
16 J. Yeon, S. H. Kim, S. D. Nguyen, H. Lee, and P. S. Halasyamani, Inorg. Chem. **51**, 2662 (2012).
17 A. A. Belik, M. Azuma, and M. Takano, Inorg. Chem. **44**, 7523 (2005).
18 R. David, H. Kabbour, S. Colis, A. Pautrat, E. Suard, and O. Mentré, J. Phys. Chem. C **117**, 18190 (2013).
19 J. Chen, L. Kang, H. Lu, P. Luo, F. Wang, and L. He, Phys. B **551**, 370 (2018).
20 H. M. Rietveld, J. Appl. Cryst. **2**, 65 (1969).
21 P. E. Blöchl, Phys. Rev. B **50**, 17953 (1994).
22 J. P. Perdew, K. Burke, and M. Ernzerhof, Phys. Rev. Lett. **77**, 3865 (1996).
23 G. Kresse, and J. Hafner, Phys. Rev. B **47**, 558 (1993).
24 G. Kresse, and J. Furthmüller, Phys. Rev. B **54**, 11169 (1996).
25 H. J. Monkhorst, and J. D. Pack, Phys. Rev. B **13**, 5188 (1976).
26 E. F. Bertaut, J. Appl. Phys. Suppl. **33**, 1138 (1962).
27 E. F. Bertaut, J. Phys. Colloques **32**, C1-462 (1971).
28 L. J. de Jongh, and A. R. Miedema, Adv. Phys. **23**, 1 (1974).
29 J. Q. Yan, S. Okamoto, Y. Wu, Q. Zheng, H. D. Zhou, H. B. Cao, and M. A. McGuire, Phys. Rev. Mater. **3**, 074405 (2019), arXiv: 1905.09365.
30 R. Zhong, T. Gao, N. P. Ong, and R. J. Cava, Sci. Adv. **6**, eaay6953 (2020), arXiv: 1910.08577.
31 R. L. Carlin, *Magnetochemistry* (Springer-Verlag, Berlin, 1986).
32 M. Soda, T. Hong, M. Avdeev, H. Yoshizawa, T. Masuda, and H. Kawano-Furukawa, Phys. Rev. B **100**, 144410 (2019).
33 L. Ortega-San Martin, J. P. Chapman, L. Lezama, J. Sánchez Marcos, J. Rodríguez-Fernández, M. I. Arriortua, and T. Rojo, Eur. J. Inorg. Chem. 1362 (2006).
34 L. Li, N. Narayanan, S. Jin, J. Yu, Z. Liu, H. Sun, C. W. Wang, V. K. Peterson, Y. Liu, S. Danilkin, D. X. Yao, D. Yu, and M. Wang, Phys. Rev. B **102**, 094413 (2020), arXiv: 2006.03356.
35 A. A. Aczel, L. Li, V. O. Garlea, J. Q. Yan, F. Weickert, M. Jaime, B. Maiorov, R. Movshovich, L. Civale, V. Keppens, and D. Mandrus, Phys. Rev. B **90**, 134403 (2014), arXiv: 1407.4098.
36 B. Lorenz, Y. Q. Wang, and C. W. Chu, Phys. Rev. B **76**, 104405 (2007), arXiv: cond-mat/0608195.
37 Y. J. Choi, H. T. Yi, S. Lee, Q. Huang, V. Kiryukhin, and S. W. Cheong, Phys. Rev. Lett. **100**, 047601 (2008).
38 R. Chen, J. F. Wang, Z. W. Ouyang, Z. Z. He, S. M. Wang, L. Lin, J. M. Liu, C. L. Lu, Y. Liu, C. Dong, C. B. Liu, Z. C. Xia, A. Matsuo, Y. Kohama, and K. Kindo, Phys. Rev. B **98**, 184404 (2018).
39 W. H. Ji, L. Yin, W. M. Zhu, C. M. N. Kumar, C. Li, H. F. Li, W. T. Jin, S. Nandi, X. Sun, Y. Su, T. Brückel, Y. Lee, B. N. Harmon, L. Ke, Z. W. Ouyang, and Y. Xiao, Phys. Rev. B **100**, 134420 (2019), arXiv: 1905.06282.
40 S. Dong, J. M. Liu, and E. Dagotto, Phys. Rev. Lett. **113**, 187204 (2014), arXiv: 1410.2682.
41 K. Du, L. Guo, J. Peng, X. Chen, Z. N. Zhou, Y. Zhang, T. Zheng, Y. P. Liang, J. P. Lu, Z. H. Ni, S. S. Wang, G. Van Tendeloo, Z. Zhang, S. Dong, and H. Tian, npj Quantum Mater. **5**, 49 (2020), arXiv: 2007.12828.